On the Design of Gigabit Indoor Wireless LANs at 60 GHz

I. D. Holland, W. G. Cowley, and C. Burnet

Institute for Telecommunications Research *
University of South Australia
Mawson Lakes Blvd., Mawson Lakes, SA, 5095.
{ian.holland,bill.cowley,craig.burnet}@unisa.edu.au

Abstract

We consider issues related to the design of a 60GHz short-range wireless local area network (WLAN) using low cost components and aiming at data rates on the order of 1Gbit/s. It is anticipated that the use of adaptive modulation and coding (AMC) in conjunction with orthogonal frequency division multiplexing (OFDM) will be an effective multipath resistant strategy. It is desired to keep the number of sub-carriers low so as to limit the degradation due to practical issues such as phase noise. As the feasibility of this approach depends on the multipath propagation characteristics likely to be encountered, we present a 3D ray tracing approach for obtaining complex-valued channel impulse responses for a target environment consisting of a typical small/medium office or small lab. Using this approach, a number of impulse responses have been obtained via Monte Carlo simulation. These responses were then used in obtaining preliminary predictions of the throughput that could be expected if an AMC-OFDM scheme was to be implemented in the target environment. Albeit under some simplifying assumptions, the results suggest that for a large number of possible transmitter and receiver placements, data rates on the order of a gigabit per second are possible.

1. Introduction

In recent years, there has been a growing interest in developing technologies for the support of high data rate services in wireless networks. Large research consortiums such as WIGWAM [1], [2], are focusing on the development of wireless systems capable of achieving up to 1Gbit/s using carrier frequencies in multiple bands. Whilst the main band considered in the WIGWAM project is the 5GHz band [1], the license free availability of a large amount of continuous bandwidth in the 60GHz band and the high interference isolation at these frequencies has made this band a viable option for use in achieving data rates exceeding 1Gbit/s in short-range indoor wireless local area networks. Efforts in the standardisation of the millimeter-wave (mm-wave, which includes the 60GHz band) physical layer are ongoing within IEEE 802.15.3 Task Group c. Early work conducted in Australia regarding the development of wireless local area networks using OFDM and operating at mm-wave frequencies was presented in [3], with a prototype design of a 40GHz system having a raw link rate of 54Mbit/s being described. The current paper discusses aspects related to the modem design and preliminary results we have obtained as part of a recent Australian research effort supported by an ARC Linkage Grant that aims at building a prototype mm-wave wireless system [4] (in the 60GHz band) for achieving data rates on the order of gigabits per second, with low cost components as would be important for consumer applications.

For data rates at or above 1Gbit/s, root mean square (RMS) delay spreads on the order of nanoseconds result in a high degree of frequency selectivity. Therefore, the use of OFDM in conjunction with an AMC strategy is expected to be an effective transmission scheme. More specifically, subcarriers experiencing a sufficiently high signal-to-noise ratio (SNR) can be assigned a higher code rate and/or a higher order signal constellation, whilst the use of a sufficiently low modulation and coding rate would ensure reliable data transfer over subcarriers experiencing a lower SNR. However, many practical issues must be considered in designing such a system. Such issues include for instance the effects of phase noise, as well as time/frequency synchronisation errors. Whilst such issues will not be explicitly investigated in this paper, they are noted as motivating the desire to keep

*This work was supported by the Australian Research Council and NHEW R&D Pty. Ltd.

the number of sub-carriers low in the OFDM system. The number of sub-carriers used in obtaining the results in this paper has been chosen as 16. The feasibility of using this small number of sub-carriers is largely dependent on the nature of the multipath propagation that would typically be encountered for the short-range indoor WLANs envisaged for the 60GHz band. It has been noted [5] that in this band, both the penetration loss and the attenuation due to reflections involving typical home/office materials is quite large. Furthermore, the propagation loss at 60GHz is very high. Due to the large propagation and penetration losses, 60GHz WLANs are primarily intended for use in short-range, single room environments. Moreover, due to the large reflection losses, a reasonable approximation of the channel impulse response can be obtained by considering only the first order reflections (i.e. no paths involving multiple reflections are considered) and where applicable a line-of-sight (LOS) path between the transmitter and receiver [5].

2. System Model

A block diagram for an AMC-OFDM system is shown in Fig. 1. Briefly, the input data stream is coded and then mapped to an M-ary phase shift keying (PSK) constellation, determined by a threshold comparison with the estimated E_s/N_0 for each sub-carrier. More specifically, a lower E_s/N_0 threshold would be defined for activating each modulation and coding scheme. These thresholds should be to chosen in a manner that ensures that a targeted level of reliability (e.g. a target bit error rate) could be achieved. Assuming N sub-carriers, an N-point inverse fast Fourier transform (IFFT), as well as the indicated serial-to-parallel (S/P) and parallel-to-serial (P/S) operations, is then used in forming the set of OFDM symbols to be transmitted. Note that the addition of the cyclic prefix is done so as to mitigate the effects of inter-carrier and inter-symbol interference that would otherwise be experienced due to the time-dispersive nature of the multipath channel. The duration of the cyclic prefix should be no less than the length of the channel impulse response, in order to fully mitigate these effects. The model for the multipath channel will be discussed in Section 3.. Prior to transmission, digital-to-analog (D/A) conversion is simulated for each of the in-phase (I) and quadrature (Q) components of the OFDM signal. In order to accurately model the performance of the proposed system, it is important to explicitly include the effects of the clipping and quantisation operations that are performed during D/A conversion. Hence, these operations are also included in the block diagram. Similarly, at the receive side, clipping and quantisation are included since these operations would be performed in the analog-to-digital (A/D) converters for the I and Q components of the received signal. The OFDM demodulation procedure is performed by stripping off the cyclic prefix and performing an N-point fast Fourier transform (FFT), along with the indicated S/P and P/S operations. The output data stream would then be obtained following PSK constellation demapping and decoding.

It should be noted that in this paper, the AMC-OFDM scheme has not been explicitly simulated. Rather, simulations are conducted using uncoded quadrature phase shift keying (QPSK), in order to obtain E_s/N_0 estimates for each sub-carrier. By counting the number of sub-carriers having estimated E_s/N_0 lying between the thresholds of each mode, the achievable throughput can be predicted. In this paper, a genie-aided channel estimation method is assumed, whereby for the purposes of estimating the amplitude attenuation and phase shift on each sub-carrier, the transmitted data is assumed to be known. The complex-valued channel estimate affecting each transmitted symbol on each sub-carrier is then obtained simply by dividing the received symbols (after the FFT block) by the transmitted symbols. Moreover, the E_s/N_0 estimation uses the single sample-per-symbol version of the data-aided maximum likelihood SNR estimator described in [6], with the genie-known transmitted symbols and the phase-compensated received symbols on each sub-carrier. Practical approaches for channel estimation suitable for the gigabit WLAN modems are currently under investigation. Other practical issues such as time/frequency synchronisation and phase noise are also being investigated.

3. Channel Model

3.1. 3D ray tracing approach

In obtaining the channel impulse response for a given indoor scenario, a 3D ray tracing approach is applied. Our preliminary studies have determined that for transmission in the 60GHz band, the phase changes in reflections and also the phase shifts due to path differences should not be neglected. Therefore, these effects are incorporated in the proposed ray tracing approach.

Assume vertically polarised transmit and receive antennas aligned with the z-axis of a right-handed cartesian coordinate system. Then, the proposed 3D ray tracing approach can be summarised by the following procedure. First, the vectors defining each of

the possible paths from the transmitter to the receiver are determined. Next, the normalised electric field (E-field) intensity vector for each path is calculated. For all paths involving a reflection, it is necessary to first determine the E-field intensity vector for the wave incident on the reflector. Assume a dipole transmit antenna aligned in the z (i.e. vertical) direction with reference to the right-handed cartesian coordinate system. Then, the basis vector defining the direction of the E-field intensity can be obtained in terms of standard cartesian basis vectors $\hat{\mathbf{e}}_x$, $\hat{\mathbf{e}}_y$, $\hat{\mathbf{e}}_z$, as [7]

$$\begin{aligned}\hat{\mathbf{e}}_\theta = &\frac{x'z'}{\sqrt{(x'^2+y'^2)\,(x'^2+y'^2+z'^2)}}\hat{\mathbf{e}}_x \\ &+\frac{y'z'}{\sqrt{(x'^2+y'^2)\,(x'^2+y'^2+z'^2)}}\hat{\mathbf{e}}_y \\ &-\frac{\sqrt{x'^2+y'^2}}{\sqrt{x'^2+y'^2+z'^2}}\hat{\mathbf{e}}_z.\end{aligned} \tag{1}$$

where (x', y', z') denote the coordinates of the reflector relative to the transmitter. The incident E-field intensity vector is now found (for the assumed case of a vertical dipole transmit antenna) as [8]

$$\mathbf{E}_i = \left[\frac{\cos\left(\frac{\pi}{2}\cos\theta\right)}{\sin\theta}\right]\hat{\mathbf{e}}_\theta, \tag{2}$$

where the free space path loss and the phase shift associated with propagation have not yet been included, but will be accounted for in determining the E-field intensity at the receiving antenna. Also, it should be noted that the transmit antenna gain will be included in Section 3.3..

In order to determine the E-field intensity vectors for each of the reflected waves, the incident E-field intensities are decomposed into parallel and perpendicular polarised components (with respect to the plane of incidence). Based on a procedure outlined in [9], this is achieved as follows. Initially, unit vectors in the directions of the perpendicular and parallel E-field components are found as

$$\hat{\mathbf{e}}_{i,\perp} = \frac{\mathbf{u}_i \times \mathbf{n}_s}{|\mathbf{u}_i \times \mathbf{n}_s|}, \tag{3}$$

$$\hat{\mathbf{e}}_{i,\parallel} = \frac{\hat{\mathbf{e}}_{i,\perp} \times \mathbf{u}_i}{|\mathbf{u}_i|}, \tag{4}$$

where $\mathbf{n}_s$ is a unit vector normal to the surface of incidence, and

$$\mathbf{u}_i = x'\hat{\mathbf{e}}_x + y'\hat{\mathbf{e}}_y + z'\hat{\mathbf{e}}_z \tag{5}$$

denotes the path vector for the incident wave. Also, $\times$ denotes the cross product operator. The perpendicular and parallel components of the incident E-field intensity are then found as

$$E_\perp = \hat{\mathbf{e}}_{i,\perp} \cdot \mathbf{E}_i, \tag{6}$$

$$E_\parallel = \hat{\mathbf{e}}_{i,\parallel} \cdot \mathbf{E}_i, \tag{7}$$

where $\cdot$ denotes the dot product operator. The E-field intensity vector for the reflected wave is given by

$$\mathbf{E}_r = E_\perp R_\perp \hat{\mathbf{e}}_{i,\perp} + E_\parallel R_\parallel \hat{\mathbf{e}}_{r,\parallel}, \tag{8}$$

where the unit vector in the direction of the parallel polarised reflected component is given by

$$\hat{\mathbf{e}}_{r,\parallel} = \left(\mathbf{n}_s \cdot \hat{\mathbf{e}}_{i,\parallel}\right)\mathbf{n}_s - \left[\left(\mathbf{n}_s \times \hat{\mathbf{e}}_{i,\perp}\right) \cdot \hat{\mathbf{e}}_{i,\parallel}\right]\left(\mathbf{n}_s \times \hat{\mathbf{e}}_{i,\perp}\right). \tag{9}$$

Also in (8), $R_\perp$ and $R_\parallel$ denote the reflection coefficients for the perpendicular and parallel components, respectively. Details on the calculation of these reflection coefficients will be given in Section 3.1.1.. It should be noted that these coefficients are typically complex valued and thus (8) incorporates both the amplitude attenuation and the phase shift due to reflection.

Having determined the E-field intensity vectors for each of the reflected waves, the corresponding E-field intensity of the reflected wave incident on the receiver needs to be determined. Therefore, accounting for the free space loss with respect to the line-of-sight (LOS) path, and the phase shift associated with propagation, the E-field intensity vector incident on the receiver from a reflected wave is given as

$$\mathbf{E}_{Rx,i,r} = \mathbf{E}_r \frac{d_{LOS}}{d_{ref}} \exp\left[-j\left(\frac{2\pi}{\lambda}\right)d_{ref}\right], \tag{10}$$

where d_{LOS} denotes the distance of the LOS path, d_{ref} denotes the total distance of the reflected path, and λ is the carrier wavelength. Note that the phase shift associated with propagation is preserved in the term $\exp\left[-j\left(\frac{2\pi}{\lambda}\right)d_{ref}\right]$, as done, for instance, in [10]. Note that the E-field incident on the receiver due to the LOS component is assumed to be normalised so that it would have unit magnitude in the case where the transmit and receive antennas were of the same height, and would therefore be given by

$$\mathbf{E}_{Rx,i,LOS} = \left[\frac{\cos\left(\frac{\pi}{2}\cos\theta\right)}{\sin\theta}\right]\exp\left[-j\left(\frac{2\pi}{\lambda}\right)d_{LOS}\right]\hat{\mathbf{e}}_\theta, \tag{11}$$

where θ and $\hat{\mathbf{e}}_\theta$ are now defined with respect to the direction of the LOS wave and the transmit antenna alignment (which has been assumed as in the z-direction). It is noted that the term $\left[\frac{\cos\left(\frac{\pi}{2}\cos\theta\right)}{\sin\theta}\right]$ explicitly accounts for the pattern of the vertical dipole

transmit antenna in the LOS wave, as was done in (2) for the paths involving a reflection.

Under the assumption of a vertically aligned dipole receive antenna, the complex open circuit voltages for each of the received waves are calculated as

$$V_{oc} = \mathbf{E}_{Rx,i} \cdot \left[\frac{\cos\left(\frac{\pi}{2}\cos\theta\right)}{\sin\theta} \right] \hat{\mathbf{e}}_\theta, \tag{12}$$

where θ and $\hat{\mathbf{e}}_\theta$ are now defined with respect to the incident wave, either from a reflector or directly from the transmitter for the LOS case, and the receive antenna alignment (which has been assumed as in the z-direction). Also, $\mathbf{E}_{Rx,i}$ denotes the receiver-incident E-field intensity vector for either the LOS or a reflected wave as appropriate.

The complex valued continuous-time impulse response $h_c(\tau)$, where τ denotes excess delay, is now determined as follows. For each received wave, calculate the excess delay (with respect to the LOS path), and define the value of the impulse response at that excess delay with the corresponding complex open circuit voltage induced in the receiving antenna due to that wave. It now remains to determine the equivalent discrete-time impulse response $h[k] = h_c(t) * h_o(t)|_{t=k/f_s}$, where f_s denotes the sampling rate, $h_o(t)$ denotes the combined impulse response of the transmit and receive filters, and where it is assumed that the receiver samples are taken at time instants $t = [1/f_s, 2/f_s, \ldots]$. Note that a single sample per symbol is assumed, and therefore f_s equals the symbol rate R_s. Further, note that $t = 0$ is defined as the time at which the received pulse due to the LOS wave begins. Assuming that the D/A converter results in a square pulse of duration $T_s = 1/f_s$ for each symbol, and that the anti-aliasing filter at the Rx is matched to the transmit pulse, the pulse shape due to a single multipath component will be triangular, with a width of $2T_s$. Thus, the overall impulse response of the transmit and receive filters is specifically defined as

$$h_0(t) = \begin{cases} 0; & t < 0, \\ t/T_s; & 0 \le t \le T_s, \\ 2 - t/T_s; & T_s \le t \le 2T_s, \\ 0; & t \ge 2T_s. \end{cases} \tag{13}$$

The discrete-time equivalent impulse response of the channel, taking into account the effects of the transmit and receive filters, is then given by

$$h[k] = \sum_{i=1}^{N_p} h_i h_0\left(kT_s - \tau_i\right), \tag{14}$$

where N_p denotes the number of multipath components arriving at the receiver, h_i denotes the complex weight of the i^{th} component, and τ_i denotes the excess delay for that component.

3.1.1. Reflection coefficients

In determining the reflection coefficients for use in (8), it is assumed that all reflections occur from smooth, planar surfaces. In this case, the reflection coefficients are found as [10]

$$R_\perp = \frac{\cos\left(\pi/2 - \psi_{in}\right) - \sqrt{\epsilon - \sin^2\left(\pi/2 - \psi_{in}\right)}}{\cos\left(\pi/2 - \psi_{in}\right) + \sqrt{\epsilon - \sin^2\left(\pi/2 - \psi_{in}\right)}}, \tag{15}$$

$$R_\parallel = \frac{\epsilon\cos\left(\pi/2 - \psi_{in}\right) - \sqrt{\epsilon - \sin^2\left(\pi/2 - \psi_{in}\right)}}{\epsilon\cos\left(\pi/2 - \psi_{in}\right) + \sqrt{\epsilon - \sin^2\left(\pi/2 - \psi_{in}\right)}}, \tag{16}$$

where ψ_{in} is defined as the angle of incidence. More specifically, this angle is measured within the plane of incidence, between the incoming wave and the surface of incidence. Also, ϵ denotes the complex dielectric constant for the reflecting surface, which is defined as [11]

$$\epsilon = \epsilon_r - j\epsilon_r \tan\left(\delta\right), \tag{17}$$

where ϵ_r is the relative dielectric constant, and $\tan(\delta)$ denotes the loss tangent. For a carrier frequency of 60GHz, these values are tabulated for some common building materials in [11].

3.2. Indoor scenarios for 60GHz

The 3D ray tracing approach described in Section 3.1. has been applied to two specific indoor scenarios, in order to obtain sample impulse responses for use in simulations (see Section 4.) of the proposed system. In each scenario, only paths involving a single reflection, and an LOS path, are included. To account for the situation where the LOS path is blocked, it is possible to specify an attenuation of the LOS path component. Effects such as diffraction due to edges and corners, have not been included at this stage. It has been noted in [12] that the diffraction effects at 60GHz are not typically significant.

The first considered scenario is a bench top model, which corresponds to the situation where the transmitter and receiver are located on the same bench within an office of height 2.7m, width 2.9m, and length 4.9m (chosen to match the dimensions of the first author's office). The bench is assumed to be of length 3m and may lie anywhere along the longest wall. A cross-sectional plan view looking from the ceiling towards the bench

top is shown in Fig. 2. Since only the LOS path and the first-order reflections are included in the ray tracing, there will be four wall reflections and an LOS path (as indicated in Fig. 2). Additionally, there will be a reflected path from the bench top, and a reflected path from the ceiling. These paths are not explicitly shown on the diagram, but are included in the model. The geometrical parameters for the bench top model are assumed to be uniformly distributed on the intervals defined as follows. The transmitter (Tx) and receiver (Rx) heights are between 5cm and 30cm, the distances from the Tx and Rx to the wall along which the bench lies are between 10cm and 1m. Given the distance $d_{T-R,b}$, defined as the distance along the edge of the bench between the Tx and Rx, and assumed to be uniformly distributed between 1m and 3m, the distance d_{T-LW} between the Tx and the wall on the left hand side of the diagram is assumed to be uniformly distributed on the interval $[0.1m, 4.8m - d_{T-R,b}]$. All remaining parameters used in determining the path vectors are deterministic given the room geometry and the aforementioned other geometrical parameters.

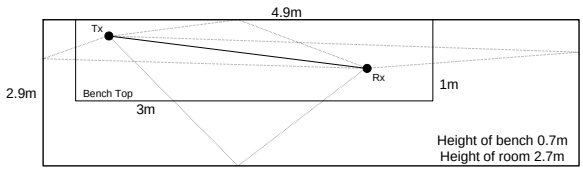

Figure 2: Plan view for the bench top model.

The second scenario is an empty room model, with the same room dimensions as for the bench top model. The main difference between the bench top model and the empty room model is in the aforementioned restrictions placed on the positioning of the Tx and Rx in the bench top model. In the empty room case, the only restrictions on the placement of the Tx and Rx is that they must be at least 0.05m from the nearest reflecting surface, and that the distance between the Tx and Rx, projected along the longest wall, is at least 0.05m. The possible paths are the same as in the bench top model, except that instead of a bench reflected path, there is now a floor reflected path. Note that where applicable in each of the aforementioned scenarios, it is assumed that the walls and the ceiling are made of plasterboard, and that the bench top and floor are wooden.

3.3. Example link budget

Due to the method of normalisation used in defining the channel impulse response in Section 3.1., it remains to account for the antenna gains, the free space loss encountered for the LOS path, as well as other system losses. These factors are accounted for in the link budget. Assuming a transmitted symbol rate of 1Gsym/s and vertical dipole antennas for both Tx and Rx, an example link budget for the LOS path is shown in Table 1. It should be noted that the stated E_s/N_0 value of 8.32dB was calculated under the assumption that Tx and Rx antennas were of the same height, and separated by the stated reference distance of 3m. Whilst any differences in antenna heights will already be accounted for within the impulse response defined as in Section 3.1., the E_s/N_0 value is scaled to account for the actual distance of the LOS path.

Table 1: Example link budget for the LOS path.

Carrier freq.	60 GHz
Link distance	3 m
Tx power	4 mW
Tx gain	2 dBi
Tx EIRP	-18.0 dBW
System temp.	1200 deg K
Rx gain	2 dBi
Rx G/T	-28.8 dB/K
Other losses	2 dB
Symbol rate	1Gsym/s
Free space loss	77.5 dB
E_s/N_0	8.32dB

4. Numerical Results

4.1. Method of performance evaluation

For the purpose of determining the expected throughputs that could be achieved for the adaptive OFDM system proposed in Section 2., simulations have been carried out for each of the indoor scenarios described in Section 3.2.. More specifically, a set of 5000 impulse responses were generated for each indoor model, and transmission over the multipath channels with these impulse responses was done for the case of $N = 16$ sub-carriers according to the system model that was described in Section 2.. For every one of the 5000 impulse responses obtained in each of the two indoor models, an E_s/N_0 estimate was obtained for the individual sub-carriers. Comparisons of these E_s/N_0 estimates were then made with a set of thresholds chosen for two example AMC-OFDM schemes (see Section 4.4.). In practice, the aforementioned thresholds would be used in selecting the modulation and coding scheme actually used on each sub-carrier; this is explained as follows. Consider a generic AMC-OFDM scheme that has a total of K available modulation and coding schemes to choose from for each sub-carrier, in addition to the option for disabling transmission on certain sub-carriers. Assuming a time-invariant channel, and denoting the

estimated E_s/N_0 for the n^{th}, $n \in [0, N-1]$, sub-carrier by $\hat{\xi}_n$, a particular modulation and coding scheme for the n^{th} sub-carrier would be selected from K available modulation/coding schemes by comparing $\hat{\xi}_n$ with a set of K pre-defined thresholds s_k, $k \in [1, K]$. This would be done according to the criterion [13]

$$\text{Selected mode} = \begin{cases} \text{No transmission}; & 0 \leq \hat{\xi}_n < s_1, \\ k; & s_k \leq \hat{\xi}_n < s_{k+1}, \\ K; & s_K \leq \hat{\xi}_n. \end{cases}$$

4.2. Choice of the cyclic prefix length

The cyclic prefix length N_c was chosen as follows. For each of the indoor models, the RMS delay spreads were individually calculated from each impulse response. Then, the mean RMS delay spread, $\bar{\tau}_{rms}$, over all 5000 impulse responses in each indoor model was calculated. The cyclic prefix length was then selected as

$$N_c = \lceil \bar{\tau}_{rms} R_s \rceil, \tag{18}$$

where $R_s = f_s = 1GHz$ is the transmitted symbol rate, which is assumed to be equal to the sampling rate as was mentioned in Section 2.. The cyclic prefix lengths obtained via this method were $N_c = 2$ for both the bench top and the empty room models, which had mean RMS delay spreads of 1.40ns and 1.88ns, respectively. Also, the RMS delay spreads for the bench top and empty room scenarios had standard deviations of 0.126ns and 1.01ns, respectively. It is noted that in some cases (particularly in the empty room scenario), some of the multipath components would escape the cyclic prefix, leading to inter-symbol interference (ISI, also known as inter-block interference) and inter-carrier interference (ICI). This would result in a reduction in the SNR. However, increasing the cyclic prefix length would lead to a reduction in the achievable data rate (due to the additional overhead). Moreover, it has been noted, for instance in [14], that the SNR reduction due to ICI and ISI is not severe in systems for which the SNR is low to begin with. In our preliminary investigations, it was determined that using a longer cyclic prefix did not significantly improve performance for the investigated indoor models. In the event that larger RMS delay spreads were to be encountered, phased arrays and/or directional antennas could be used to increase antenna gain and to reduce the effects of multipath interference. We are currently investigating such options.

4.3. Effects of clipping and quantisation

Preliminary results (not shown) have been obtained for different levels of clipping and numbers of bits in the transmitter and receiver quantisation. Based on these results, it would be advisable to use 6-bits quantisation and a clipping ratio of 3 at both the transmitter and receiver. The clipping ratio is defined [15] as the maximum amplitude that is allowed to pass without clipping to the RMS level of the signal prior to clipping. Note that it is envisaged that separate D/A converters and A/D converters would be used for the I and Q components of the transmitted and received signals, respectively. In effect, an automatic gain control system has been assumed to give the clipping ratio of 3.

4.4. Expected throughput performance for indoor 60GHz scenarios

Throughput results have been estimated for both the bench top scenario and the empty room scenario for an adaptive uncoded PSK OFDM scheme, and for an adaptive 1/2-rate coded PSK OFDM scheme. Note that the choice of a single 1/2-rate code with each of the available modulation modes of BPSK, QPSK, 8PSK, has been assumed for simplicity. The available modulation modes and the lower E_s/N_0 thresholds for activating these modes are summarised in Table 2. For the uncoded case, the thresholds for each mode correspond to the E_s/N_0 for which the bit error rate would be equal to 10^{-6} for an AWGN channel. For the coded case, the E_s/N_0 thresholds for each mode are chosen to be approximately 3dB above the minimum E_s/N_0 (determined from Shannon capacity curves) for which the corresponding information bit rate for that modulation mode with half-rate coding, could be achieved. These thresholds are only intended to give a rough estimate of the level of performance that could be achieved with the proposed system; the thresholds would in practice be chosen according to the performance of the particular codec(s) employed in the adaptive scheme.

Table 2: E_s/N_0 thresholds for modulation modes.

Modulation	Lower E_s/N_0 Thresholds	
	Uncoded	1/2-Rate Coded
BPSK	10.53dB	0.5dB
QPSK	13.54dB	3.0dB
8PSK	18.72dB	6.0dB

Figs. 3 and 4 show the cumulative distribution functions for the estimated throughputs with the aforementioned adaptive PSK OFDM schemes with and without 1/2-rate coding, in the respective indoor 60GHz scenarios of the bench top and empty room. It should be noted that as advised in Section 4.3., 6-bits quantisation and a clipping ratio of 3 have been used in the simulations from which the throughput estimates were obtained. Also, the reduction in throughput due

to the inclusion of the cyclic prefix (by a factor of $N/(N+N_c) = 16/18$) has been included in the presented results. For both the bench top and the empty room scenarios, the use of coding is seen to greatly increase the probability of achieving throughputs at or above 1Gbit/s. This occurs since in the coded cases, transmission is still allowed on sub-carriers having E_s/N_0 values as low as 0.5dB, whereas for the uncoded cases, transmissions are disallowed on all sub-carriers having $E_s/N_0 < 10.53$dB (see Table 2), resulting in a zero throughput for those sub-carriers. Since the use of coding also limits the achievable throughput to $[N/(N+N_c)] \times 1.5$Gbit/s, it would be advisable to employ a hybrid approach, whereby sub-carriers with sufficiently high E_s/N_0 values could use uncoded or higher-rate coded QPSK or 8PSK.

It is observed in the empty room case (see Fig. 4) that even for the 1/2-rate coded adaptive PSK OFDM scheme there is quite a high outage probability. More specifically, for approximately 4% of the 5000 simulated Tx/Rx placements within the room, the throughput would be zero. It turns out that a large proportion of these outages occurred when the elevation angle θ on the LOS path was far from the optimal value of 90° for vertically aligned dipoles. Typically, the Tx/Rx heights would not be completely arbitrary and therefore the results presented are seen to be somewhat conservative. Moreover, options such as phased arrays could be used to improve directionality in azimuth and/or elevation. In [16], we have presented some initial results for the case in which phased arrays are used to increase directionality in azimuth. These results were obtained for the 1/2-rate coded adaptive PSK OFDM scheme for the same bench top and empty room models presented here, and show that simple 2-element phased arrays at both the Tx and the Rx would be of benefit (allowing an approximately 4-fold reduction in required Tx power) in the considered environments. We intend to extend the investigation of the phased array approaches to ascertain the potential benefits that could be achieved when using the phased arrays to steer beams in elevation instead of or in addition to azimuth.

5. Conclusions

This paper has presented encouraging preliminary simulation results for a gigabit short-range wireless local area network operating at millimetre wavelengths. For a typical small/medium office environment having little or no furniture, with the example link budget parameters summarised in Table 1, it has been demonstrated that data rates exceeding 1Gbit/s could potentially be achieved with high probability when a dominant LOS path is present. Specifically, in the case where the Tx and Rx were located on the same bench, data rates of 1Gbit/s or above were predicted to be possible for approximately 90% of the Monte Carlo simulated Tx/Rx placements. In order to achieve this performance, a 1/2-rate coded adaptive PSK OFDM scheme could be used. In the case where the room is empty and the Tx/Rx placement is arbitrary, the probability of achieving data rates in excess of 1Gbit/s was only about 53%. These results were noted to be somewhat pessimistic however, since the Tx/Rx placement would not typically be arbitrary within a small/medium office or small lab environment. Moreover, if for instance a ceiling mounted transmitter was installed, it is unlikely that a vertically polarised (with respect to the room geometry) Tx antenna would be chosen, since this would dramatically reduce the signal strength in the direction of receivers having typical heights.

Of course, the performance predictions in this paper were obtained without including practical effects such as imperfect channel estimation, phase noise, amplifier non-linearities, or imperfect time/frequency synchronisation. Such issues are currently being explored. Further adaptive strategies to maximise throughput are also being investigated. Note that the current simulations have not explored the effects of edge and corner diffraction. However, the diffraction effects at 60GHz are typically small. We have conducted preliminary investigations into the effects of blocking the LOS and/or other paths. In the bench top case, attenuation of the LOS path by 20dB led to an increase in RMS delay spreads of a few nanoseconds, and a large reduction in SNR. In some practical scenarios, the RMS delay spreads may also be increased due to the presence of furniture or office partitions, deployment within larger rooms, or the contribution of 2^{nd} and higher order reflections. We are investigating the extent to which the use of phased arrays could improve the SNR and better cope with the detrimental effects of multipath propagation in such scenarios.

Acknowledgements

The authors acknowledge the support of the Australian Research Council (ARC) provided through an ARC Linkage Grant, as well the support of NHEW R&D Pty. Ltd, Intel Corporation, Cadence Design Systems, Jazz Semiconductor and Peregrine Semiconductor. Also, the authors wish to thank Dr. Neil Weste and Prof. Harry Green for their helpful comments.

References

[1] G. Fettweis and R. Irmer, "WIGWAM: System Concept Development for 1 Gbit/s Air Interface", in Proc. *14th Wireless World Research Forum (WWRF 14)*, San Diego, USA, July 2005.

[2] J. Ebert et. al., "Paving the way for gigabit networking", *IEEE Communications Magazine*, vol. 43, no. 4, pp. 27-30, Apr. 2005.

[3] D. J. Skellern et. al., "A mm-wave high speed wireless LAN for mobile computing - architecture and prototype modem/code implementation", in Proc. *HotInterconnects Symposium*, Stanford, USA, Aug. 1996.

[4] J. A. Howarth et. al., "60GHz radios: Enabling next-generation wireless applications", in Proc. *IEEE TENCON 2005*, Melbourne, Australia, Nov. 2005.

[5] J. Schönthier, "The 60 GHz channel and its modelling", WP3-Study, BROADWAY IST-2001-32686, version V1.0, May 2003, available: http://www.ist-broadway.org/public.html

[6] D. R. Pauluzzi and N. C. Beaulieu, "A comparison of SNR estimation techniques for the AWGN channel", *IEEE Trans. Commun.*, vol. 48, no. 10, pp. 1681-1691, Oct. 2000.

[7] D. K. Cheng, *Field and Wave Electromagnetics*, Reading: Addison-Wesley, 1989.

[8] R. C. Johnson, *Antenna Engineering Handbook*, New York: Mc-Graw Hill, 3^{rd} edition, 1993.

[9] D. I. Laurenson, *Indoor Radio Channel Propagation Modelling by Ray Tracing Techniques*, PhD. Dissertation, The University of Edinburgh, available: www.see.ed.ac.uk/˜dil/thesis.ps

[10] K. Kimura and J. Horikoshi, "Prediction of millimeter-wave multipath propagation characteristics in mobile radio environment", *IEICE Transactions of Electronics*, vol. E82-C, no. 7, pp. 1253-1259, July 1999.

[11] L. M. Correia and P. O. Françês, "Estimation of materials characteristics from power measurements at 60 GHz", in Proc. *IEEE Int. Symp. on Personal, Indoor and Mobile Radio Communications*, Den Haag, The Netherlands, Sept. 1994, pp. 510-513.

[12] P. F. M. Smulders and L. M. Correia, "Characterisation of propagation in 60 GHz radio channels", Electron. and Commun. Eng. J., vol. 9, no. 2, pp. 73-80, Apr. 1997.

[13] I. D. Holland, "Effective explicit and implicit link adaptation strategies for wireless communications", PhD Thesis, Curtin University of Technology, Australia, Dec. 2004.

[14] M. Batariere, K. Baum, and T. P. Krauss, "Cyclic prefix length analysis for 4G OFDM systems", in Proc. *IEEE Veh. Tech. Conf.*, Los Angeles, USA, Sept. 2004, pp. 543-547.

[15] K. R. Panta and J. Armstrong, "Effects of clipping on the error performance of OFDM in frequency selective fading channels", *IEEE Trans. Wireless Commun.*, vol. 3, no. 2, pp. 668-671, Mar. 2004.

[16] N. Weste et. al., "mm-wave systems for high data rate wireless consumer applications", in Proc. *Australian Conf. on Wireless Broadband and Ultra Wideband Commun.*, March 2006, Sydney, Australia, *to appear*.

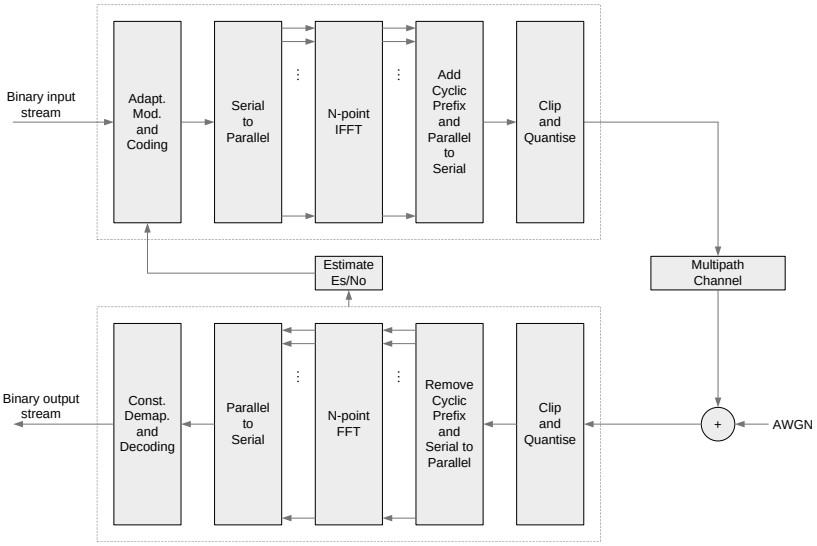

Figure 1: An OFDM system with adaptive modulation and coding.

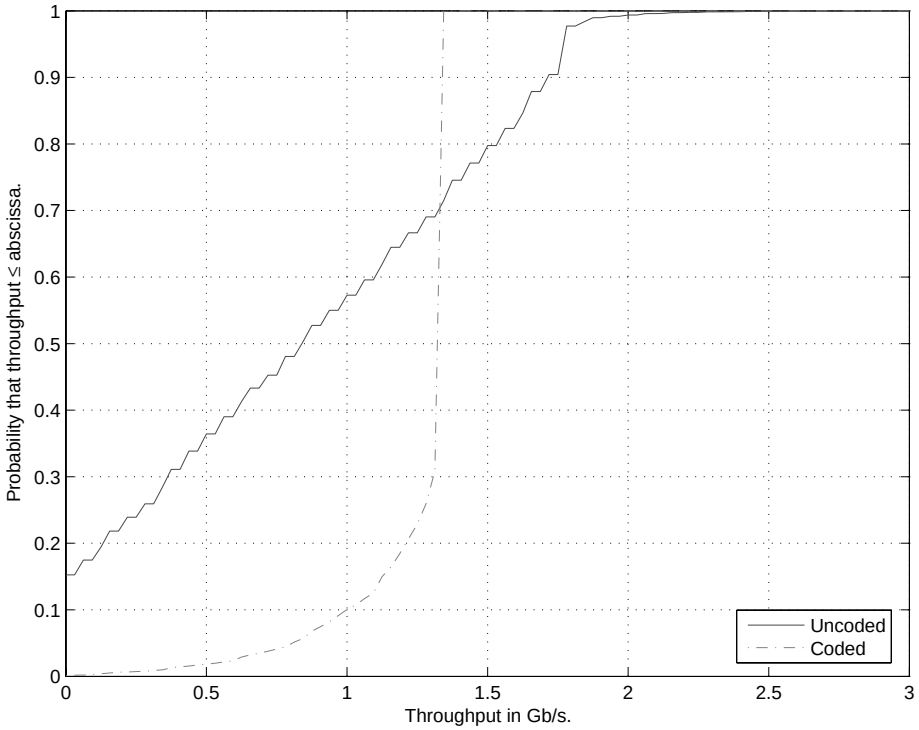

Figure 3: Cumulative distribution function of throughput for the bench top model.

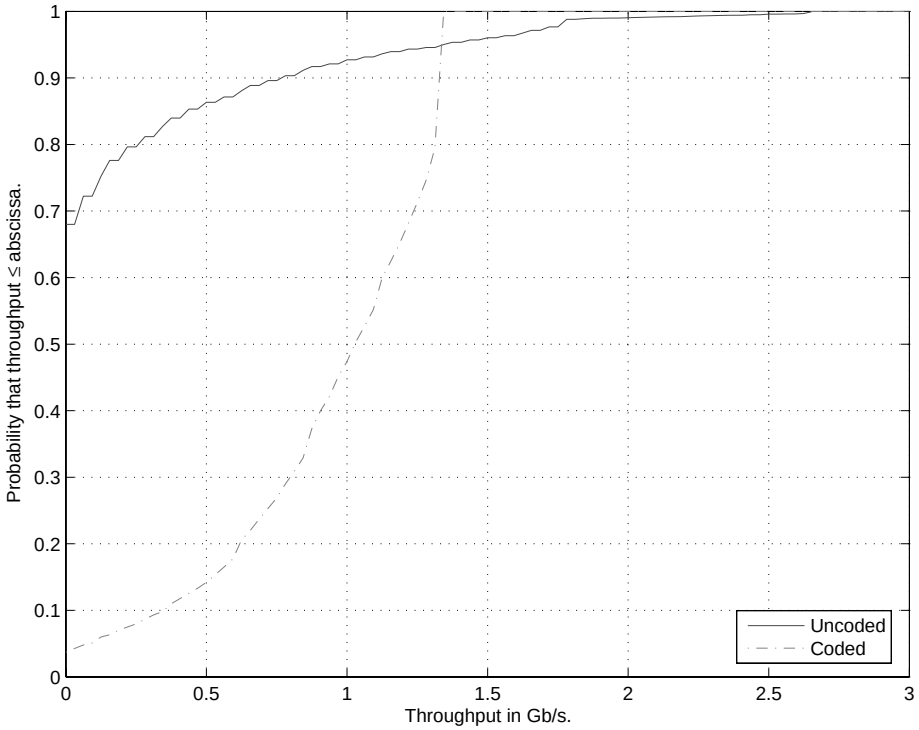

Figure 4: Cumulative distribution function of throughput for the empty room model.